J. Chem. Sci. (2020)132:140
https://doi.org/10.1007/s12039-020-01846-6

REGULAR ARTICLE

Synthesis, crystal structure, DFT calculation and trans → cis isomerisation studies of bipyridyl ruthenium(II) complexes bearing 8-oxyquinolate azo ligands

ROUMI PATRA, AMIT MAITY and KAJAL KRISHNA RAJAK*
Inorganic Chemistry Section, Department of Chemistry, Jadavpur University, Kolkata 700032, India
E-mail: kajalrajak@gmail.com

MS received 25 June 2020; revised 12 August 2020; accepted 17 August 2020

Abstract. Two stable Ru(II) bipyridyl complexes were synthesized with the deprotonated forms of the azo ligands of 8-hydroxyquinoline (hq) as analogues and they were chromatographically separated. The extended azo ligands coordinated as a bidentate ligand and chelates to ruthenium(II) through 8-quinolinolate moiety, leaving the azo part free from coordination. The general formula of the complexes are $[Ru(bpy)_2(q)]^+$. Here, q− is the deprotonated form of 5-phenylazo-8-hydroxyquinoline (Hq^1) and 5-(2-naphthylazo)-8-hydroxyquinoline (Hq^2). The complexes were verified by ^1H NMR, ESI-mass, absorption-emission spectra, cyclic voltammetry and single-crystal X-ray structure determination. UV light-induced trans → cis isomerization and reverse isomerism i.e. cis → trans around -N=N- bond at room temperature were proposed from the UV-Vis spectral changes as well as the changing of the colour of the solution of the complexes. In aid of understanding the electronic charge distribution and charge-transfer properties, computational studies employing DFT and TDDFT method have been executed.

Keywords. 8-Quinolinolato Ru(II)bipyridyl complexes; crystal structure; free azo moiety; photo isomerization; theoretical calculation.

1. Introduction

During the last two decades, a large number of reports have been published focusing on the design and characterization of the ligands and complexes with the free azo ligand moiety. The important objective is that they can serve as molecular switches,[1,2] since they can exist in two forms, namely the more stable trans (E) and the less stable cis (Z) isomers through rotation against the azo bond in the presence of photonic irradiation[3–7] which could inter-convert both photochemically or thermally. Therefore, they are excellent units to build molecular devices. Photochemical structural changes in transition metal complexes have been well-known and the photo-isomerization behavior of azo ligands in combination with a variety of transition metals (Rh, Ru, Ir) have been investigated in recent years.[8–15]

The research on ruthenium polypyridine complexes has been fascinating considering their redox stability, catalytic properties[16–18] photo-electrochemical activity under solar radiation,[19–21] non-linear optics phenomenon,[22,23] water oxidation/reduction catalysts,[24–26] molecular probe for DNA structure,[27–31] sensors[32–34] and electrochemical structure changes.[35] On the other hand, incorporation of bifunctional 8-quinolinolate fragments toward ruthenium precursors[36] results in versatile applicability of ruthenium complexes *viz.,* catalyst for nitroarene reduction,[37] antitumor and anticancer reagent.[38–40] The molar absorption coefficients can enhance significantly due to the presence of extended π-conjugations in the free azo appended 8-quinolinolate moiety. Thus, the inclusion of a photoresponsive π-conjugation component at the 5 – position of 8-quinoline is expected to be a promising approach to synthesize the photo-assisted isomeric species that may be quite valuable as model systems for theoretical studies.[41]

In this connection, we aimed to investigate reversible trans-cis isomerization study of the ruthenium

*For correspondence

Electronic supplementary material: The online version of this article (https://doi.org/10.1007/s12039-020-01846-6) contains supplementary material, which is available to authorized users.

Published online: 20 October 2020

complexes around free azo functional groups by utilizing the above-mentioned properties. Thus, the current contribution describes the synthesis, molecular structures and photophysical properties of two stable 8–Quinolinolato Ru(II) complexes of general formula [Ru(bpy)2($q^{1,2}$)](PF6) where q^1 is 5-phenylazo-8-hydroxyquinolate anion and q^2 is 5-(2-naphthylazo)-8-hydroxyquinolate anion. DFT and TD-DFT calculations were performed thoroughly to obtain better insight about the electronic structures of the complexes and to correlate experimental and theoretical interpretation.

2. Experimental

2.1 *Materials and synthesis*

Literature procedure[42] was followed to synthesize [$Ru(bpy)_2Cl_2$] and substituted 8-hydroxyquinolinearylazo[43] Hq^1- Hq^2 (general abbreviation hq). Commercially available, analytically pure chemicals and solvents were used without further purification.

2.1a Synthesis of complexes: **[$Ru(bpy)_2q^1$]PF_6,1.** A mixture of Hq^1 (50 mg, 0.20 mmol) and [$Ru(bpy)_2Cl_2$] (104 mg, 0.20 mmol) in ethanol (40 mL) with a stoichiometric amount of triethylamine was refluxed for 12 h under argon atmosphere. After cooling to room temperature, the reaction mixture was stirred with some amount of NH_4PF_6 for half an hour. Then the solvent was removed under reduced pressure. The solid product so obtained was dissolved in dichloromethane and extracted with water. Then the crude product was obtained by evaporation of the separated dichloromethane solution. The crude product was dissolved in a minimum volume of benzene and subjected to column chromatography on a silica gel column (60-120 mesh). A red band was eluted using 30% acetonitrile in benzene solution. A red coloured solid was obtained after removal of the solvent under reduced pressure. Yield: 105 mg (68%). Elemental Anal. Calcd. For [$C_{35}H_{26}N_7ORu$]PF_6: C, 65.53; H,3.97; N, 14.825. Found: C, 65.46; H, 3.79; N, 14.72 . ESI-MS (MeOH):*m/z* 662.2128 [$Ru(bpy)_2q^1$]$^+$. ^{1}H NMR {300 MHz,$CDCl_3$, δ (ppm), 9.18 (1H, d), 8.795 (1H, d), 8.427-8.350 (3H, m), 8.355 (1H, d), 8.282 (1H, d), 7.968-7.814 (7H, ArH), 7.659 (1H, d), 7.511-7.227 (11H, ArH)

[$Ru(bpy)_2q^2$]PF_6, 2. Complex **2** was synthesized using the same procedure as described for complex 1, but using Hq^2 (60 mg, 0.20 mmol).Yield: 115 mg (70%). Elemental Anal. Calcd. For [$C_{39}H_{28}N_7$-ORu]PF_6: C, 65.81; H, 3.97; N, 13.78. Found: C, 65.68; H, 3.76; N, 13.58. ESI-MS (MeOH): *m/z* 712.2376 [$Ru(bpy)_2q^2$]$^+$.^{1}H NMR {300 MHz, $CDCl_3$, δ (ppm), 9.20 (1H, d), 8.807 (1H, d), 8.402-8.357 (3H, m), 8.131 (1H, d), 7.959 (1H, d), 7.894-7.819 (7H, ArH), 7.477 (1H, d), 7.362-7.238 (13H, ArH).

2.2 *Physical measurements*

^{1}HNMR spectra were recorded on Bruker FT 300 MHz spectrometers. ESI mass spectra were recorded on a Micromass Qt of YA 263 mass spectrometer. Elemental analyses (C, H, N) were performed on Perkin–Elmer 2400 series II analyzer. Electrochemical Measurements were performed by CHI 620A electrochemical analyzer in which the potentials were referenced to the Standard Calomel Electrode (SCE) without junction correction. Absorption data were studied on a Perkin–Elmer LAMBDA 25 spectrophotometer and emission data were recorded on a Horiba FluroMax-4 fluorescence spectrometer with a slit width of 5 nm for both excitation and emission. The quantum yields were calculated by the usual method.[44] The Science tech UV light source was used for the cis-trans isomerism study. The cuvette containing ∼20 μM solution of the complexes was placed in front of the UV light source, allowing the light to be passed through a bandpass filter of appropriate wavelength range to select the light of required wavelengths. The process of isomerisation was studied by the colour change of the solution.

2.3 *Computational details*

The geometry optimizations were carried out in CH_2Cl_2 solvent applying DFT[45] method without any symmetry constraints with B3LYP function.[46] The characterization excited state phenomenon time-dependent density functional theory (TDDFT) was used associated with the conductor-like polarizable continuum model (CPCM).[47] Calculation approach[48] associated with the effective core potential (ECP) approximation of Hay and Wadt was used for describing the [$(5s)^2(5p)^6$] core electron for ruthenium whereas the associated "double-ξ"quality basis set LANL2DZ was used for the ($5d^6$) valence electrons of Ru(II).[49] For H atoms, we used 6-31+G basis set, for C, N and O atoms, we employed 6-311+G basis set used for the optimization of both the ground state and the lowest-lying triplet excited state geometries of all complexes. Finally, to understand the nature of excited

states involved in absorption natural transition orbital (NTO) analysis has been performed for all complexes. The figures showing in MOs, NTOs and the difference density plots were prepared by using the Gauss View 5.1 software. All the calculations were performed with the Gaussian 09 software package.[50] GaussSum 2.1 program[51] was used to calculate the molecular orbital contributions from groups or atom.

2.4 *Crystallographic studies*

Single crystals suitable for X-ray crystallographic analysis of complex 1 and complex 2 were obtained by slow diffusion of hexane into CH_2Cl_2 solution at ambient temperature. Despite our best efforts, we were unable to grow a single crystal of cis-isomer obtained after irradiation of UV-light as a gradual conversion of cis → trans-isomer took place even at very low temperature. The X-ray intensity data were collected on Bruker AXS SMART APEX CCD diffractometer (Mo K_α, λ = 0.71073 Å) at 298 K and were reduced in SAINTPLUS and empirical absorption correction was applied using the SADABS package.[52] All the structures were refined by means of full matrix least-square procedure on F^2 with anisotropic displacement parameters for all the non-hydrogen atoms. Data calculations and reductions were performed using the SHELXTL V 6.14 program package.[53] Molecular diagrams were drawn using the ORTEP[54] and Mercury[55] software. Relevant crystal data are given in Supplementary Information (Table S1).

3. Results and Discussion

3.1 *Synthesis*

Two substituted 8-hydroxyquinoline-arylazo Hq^1- Hq^2 (general abbreviation Hq) were used as a monoanionic *N*, *O* donor ligand for the preparation of the Ru(II) complexes. In order to tune the photophysical properties of the complexes azoaryl groups at the 5-position were introduced on to the 8-hydroxyquinoline moiety. It is to be noted that the choice of such ligands helps us to achieve our goal in the context of synthesis of mononuclear ruthenium(II) complexes with interesting optical properties.

The stoichiometric reaction of $[Ru(bpy)Cl]_2$(where bpy is biphenylpyridine) with appropriate Hq in boiling ethanol under argon atmosphere afforded deep violet coloured complexes of general formula [Ru(bpy)2($q^{1,2}$)](PF6) in good yield (Scheme 1).

3.2 *UV-Vis absorption and emission studies of the complexes*

Both the intense violet coloured complexes displayed very strong absorption bands in the visible region, which were assigned to MLCT transitions, t_2 (Ru) → π*(L) characteristics of the ruthenium polypyridyl complexes. Complex **1** showed MLCT absorption peaks at 516 nm, 410 nm and a broad peak around 340 nm which was slightly red-shifted to 524 nm, 416 nm and 351 nm in complex **2**. This

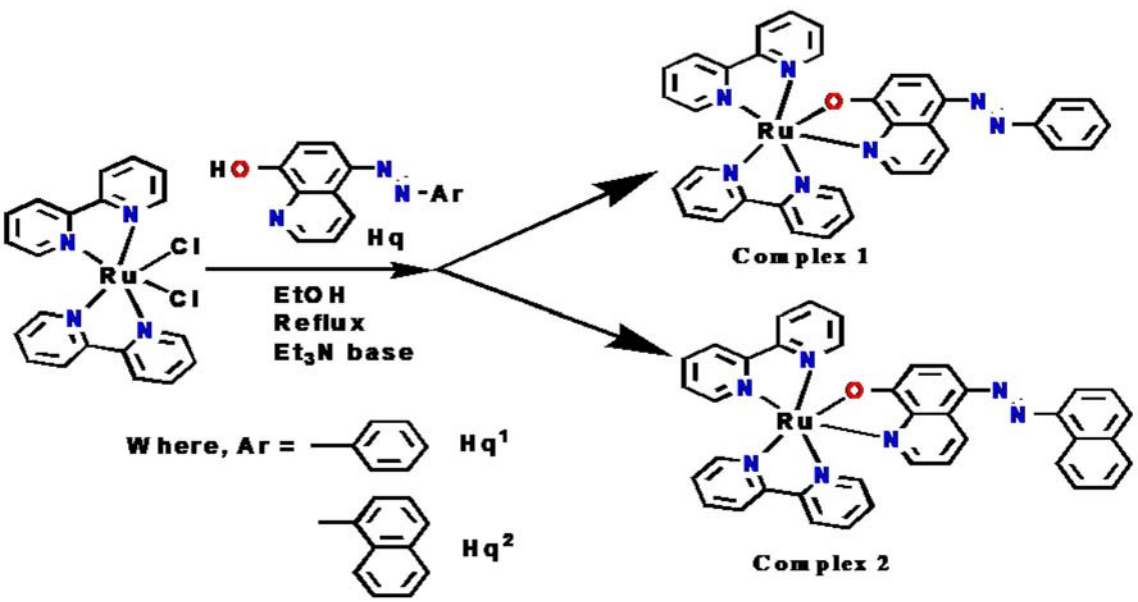

Scheme 1. Schematic representation for the synthesis of the complexes.

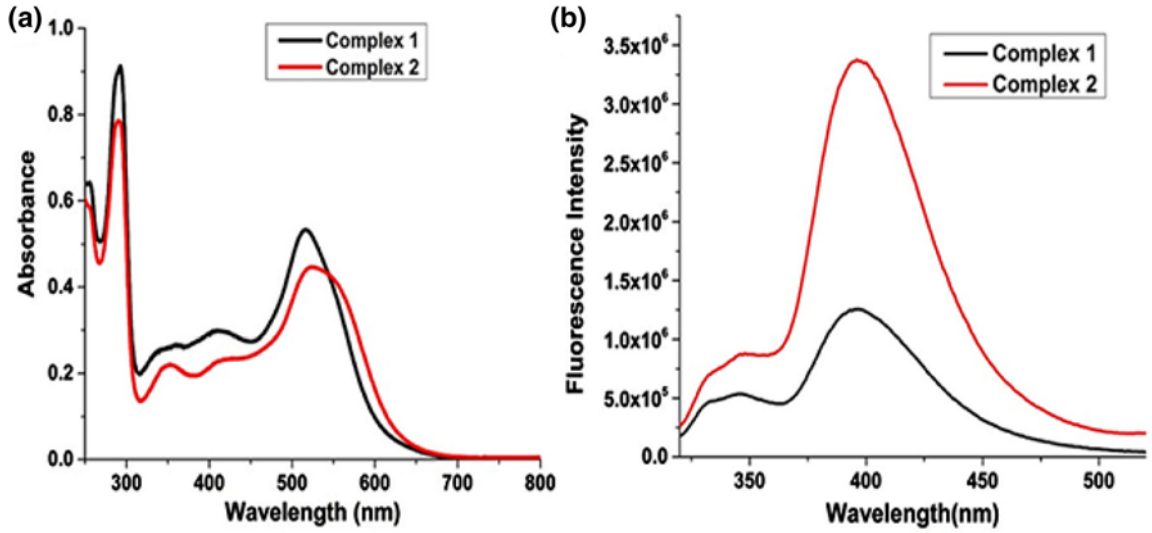

Figure 1. (a) UV-Vis spectra of the complexes (b) emission spectra of the complexes at room temperature in DCM.

bathochromic shift resulted from an increase in energy of the occupied t_{2g}-type orbital of Ru(II) in complex **2** because of extended π-conjugation. The high-energy absorption around 290 nm was assigned to be ligand-to-ligand charge transfer (LLCT and ILCT) transitions in both the complexes. Spectra are given in Figure 1.

The complexes were non-emissive when excited with low energy wavelength which was mainly related to MLCT type. But they show photoluminescence when excited with high energy ~290 nm wavelength which was entirely ligand centered LLCT and ILCT type. This data suggested ligand-based emission property. Complex **2** was around three times more emissive than complex **1**, this might be related to π extension in complex **2**. Spectra are given in Figure 1 and the photophysical properties so obtained are summarized in Table 1.

3.3 *UV-Vis absorption study of the complexes under UV light*

3.3a Complex 1: Transformation of the transisomer of complex 1 into the cis form was studied after subjecting the trans form to UV light in a controlled manner using bandpass filter at any wavelength in the range of 400-600 nm which included an MLCT transition. The trans → cis isomerism by rotation of the azo bond occurred spontaneously within 5 min when UV light was implemented on $\sim 2*10^{-5}$- (N) dichloromethane solution of the sample. The colour of the sample solution was changed immediately from violet to blue. Absorption data of the newly formed isomer was taken immediately after colour change. In the cis-isomer, the three absorption bands in the trans form shifted to longer wavelength with a decrease in intensity (new band at 628 nm, 478 nm and

Table 1. Photophysical properties of the complexes.

Complex	λ_{max}(nm)(ε(M−1cm−1))	λ_{em} (nm)	Stokes shifts (nm)	Φ_F
Complex **1**	516 (26500) 410 (15100) 340 (13300) 290 (45100)	395	105	0.08
Complex **2**	524 (22450) 416 (11600) 351 (10900) 290 (39000)	402	112	0.22

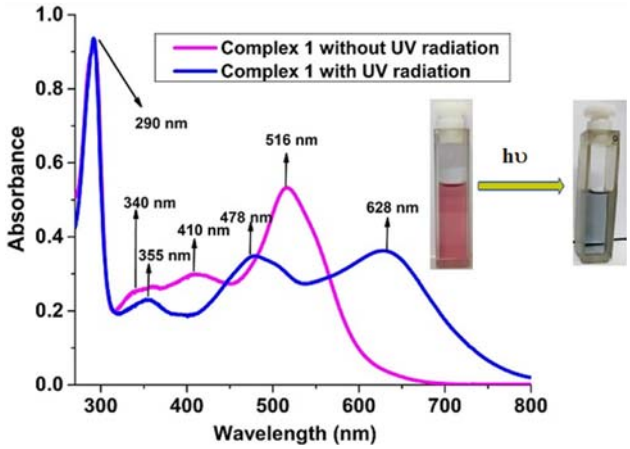

Figure 2. UV-Vis spectra of complex **1** before and after UV-radiation.

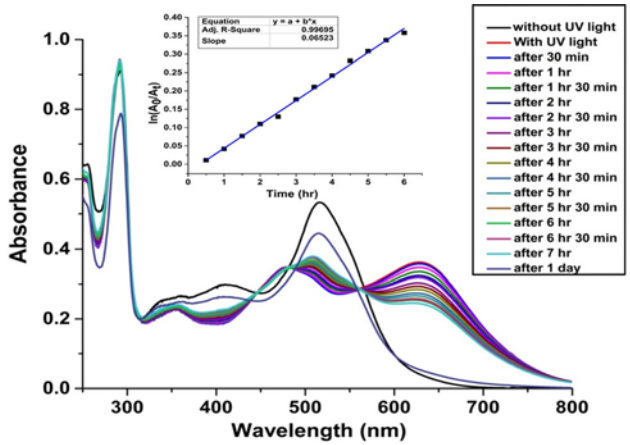

Figure 3. Time-dependent kinetic study of complex **1** in DCM for determination of stability of the cis conformer. Inset: $\ln(A_0/A_t)$ vs time (hr) plot to determine thermal cis → trans isomerisation.

355 nm) except the entirely LLCT and ILCT band at 290 nm which remained exactly in the same position. The spectra of both the isomers for complex **1** are given in Figure 2.

The cis isomer on standing in the dark undergoes reverse isomerisation with time. The time-dependent thermal kinetic study of cis → trans isomerisation has been performed in non-polar dichloromethane solution (Figure 3). Afterwards, the trans complex changed its colour to blue, the solution was thermostated in dark at room temperature and then thermal relaxation through colliding with other molecule was followed by UV-Vis spectroscopy. The complex showed relaxation time within one day. The kinetic study concluded that the stability of the cis conformer decreases gradually with time and after several hours of standing in room temperature goes back to trans conformer. The kinetic study showed that the thermal bleaching process from

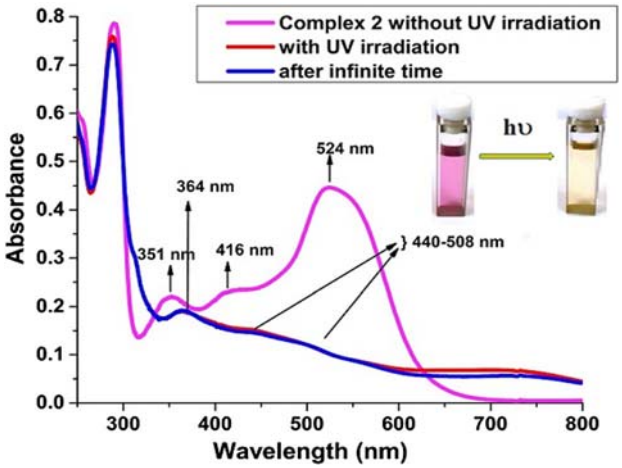

Figure 4. UV-Vis spectra of complex **2** before and after UV-radiation.

cis → trans form obeyed first-order kinetics with a rate constant $k=1.8*10^{-5}s^{-1}$ and half-life of 10.66 h in DCM at 25 °C. The kinetic study is shown in Figure 3 inset.

3.3b Complex 2: For complex **2** following the same procedure as described for complex **1**, except that changing the UV light impendent time to 15 min, we have observed a significant colour change from dark violet to light yellow. This was immediately after the observation UV-Vis spectrum was taken. And the spectrum obtained was different from the mother trans compound. From this point of view, it can be said that irradiation resulted in a new isomer and probably cis isomer of the compound. After UV light irradiation the band at 524 nm, 416 nm and 351 nm in the trans isomer vanished with a formation of a new band at 364 nm and a broadband from 440-508 nm resulted. Here also the LLCT and ILCT band around 290 nm remained unchanged (Figure 4). In the case of **2**, we have not observed reverse isomerism on standing the solution in the dark for a prolonged time. The reason is not clear. However, it is believed that the introduction of a sterically hindered bulky aryl group[56] drives the cis isomer to a higher energy excited state upon irradiation and consequently the compound decomposes.

3.4 *Cyclic voltammetry*

Electron transfer properties of the complexes were carried out in dichloromethane solution under nitrogen atmosphere at room temperature. Tetraethyl ammonium perchlorate (TEAP) as the supporting electrolyte and Pt electrode as working electrode were used. The saturated calomel electrode (SCE) without junction correction was used as a reference potential. Anodic

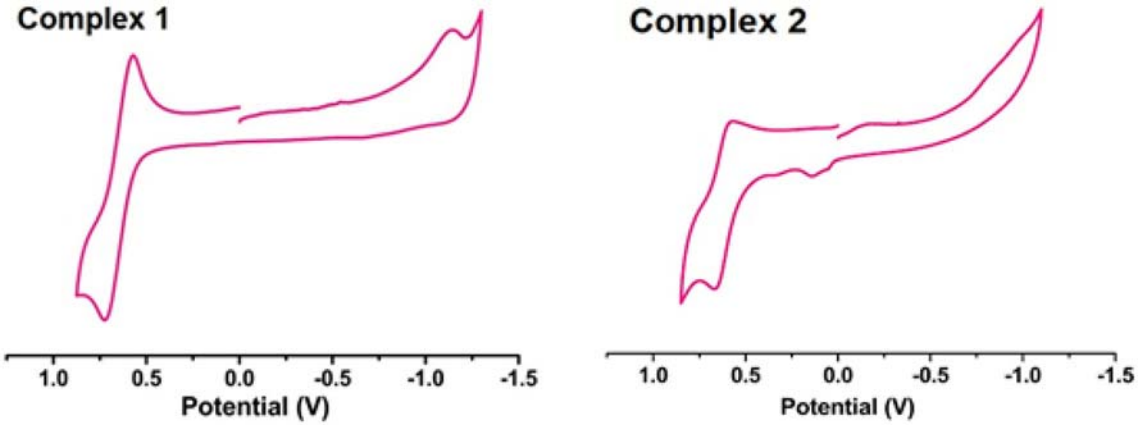

Figure 5. Cyclic voltammetric diagrams of complexes in CH_2Cl_2 at 298 K.

waves or one-electron reversible oxidation at the formal potential of +0.648 V vs SCE for complex **1** and +0.617 V vs SCE for complex **2** were observed due to Ru(II)/Ru(III)redox couple. The lower value for complex **2** might be due to the small HOMO-LUMO energy gap in complex **2**. For complex **1**, small irreversible cathodic waves at -1.14 V vs SCE resulted from the reductions of the arylazo group.[57] The absence of any peak in that region for complex **2** might be due to the presence of napthylazo ligand as a better stabilizer of ruthenium(II). The voltammograms are given in Figure 5.

3.5 *Crystal structure*

Single crystals suitable for X-ray diffraction were obtained by diffusion of hexane into dichloromethane solution at ambient temperature. The two complexes appeared as dark violet hexagonal-shaped crystals. Although geometrically the complexes seemed to be similar, but crystallographically they were different. Complex **1** crystallized with P1 space group in the triclinic crystal system and that of complex **2** asP2/c space group in a monoclinic crystal system. In complexes, 8-quinolinol bonded to the metal centre as O,

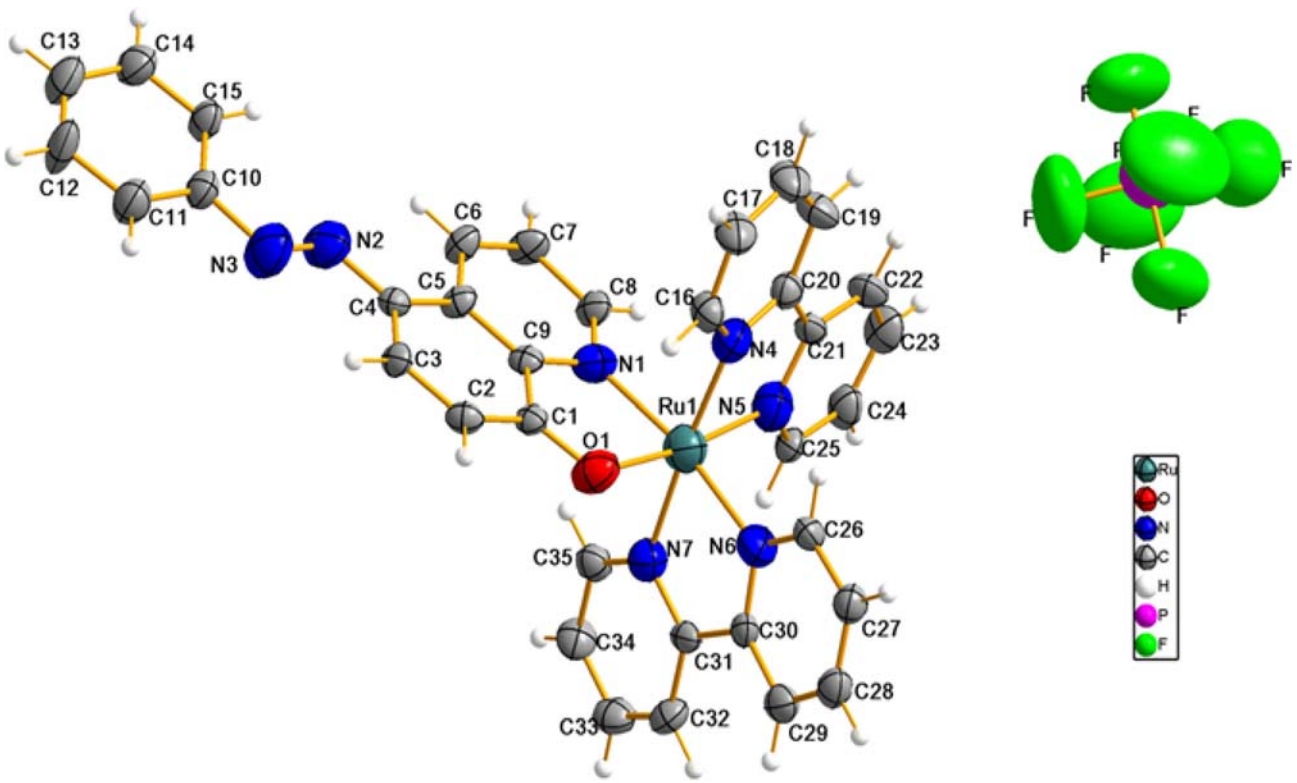

Figure 6. Molecular Ortep view of complex **1**.

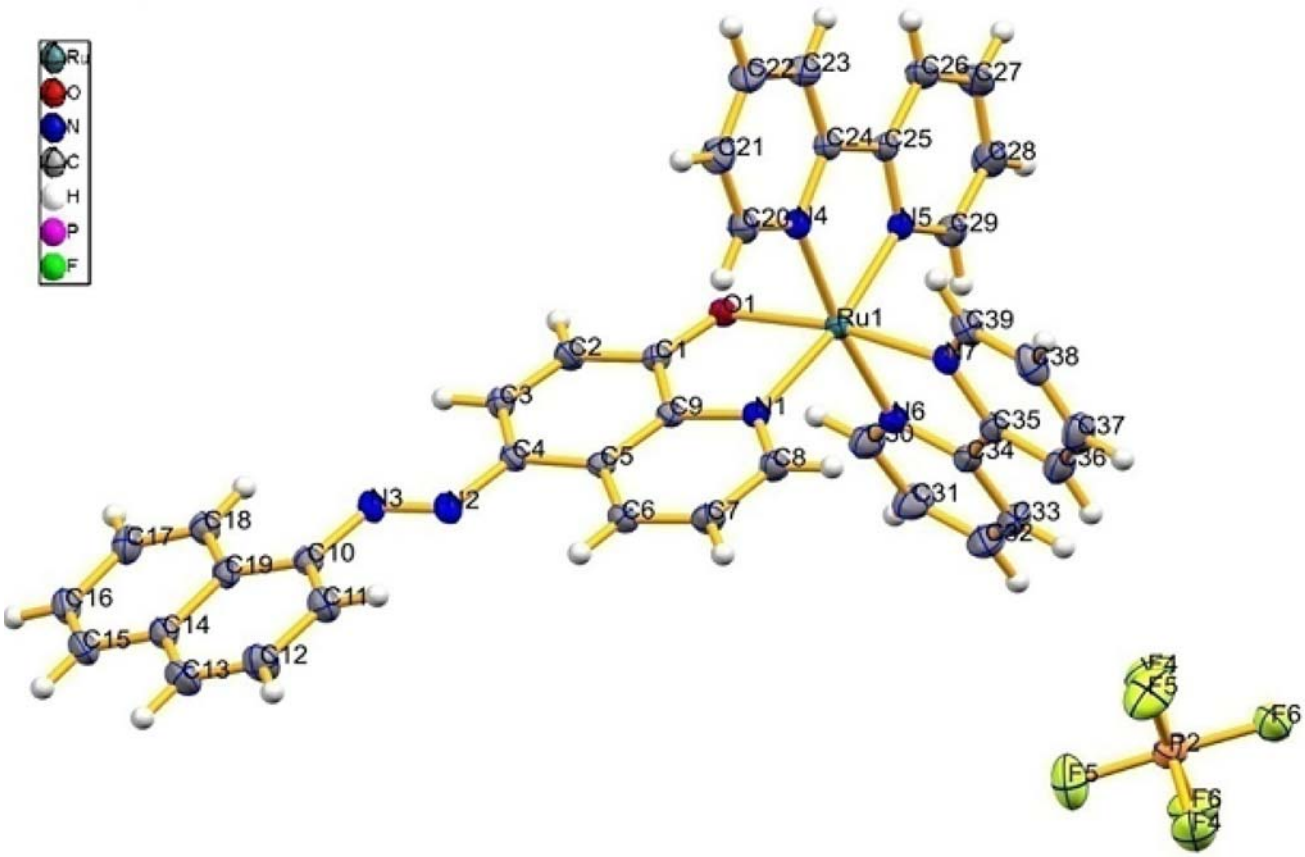

Figure 7. Molecular Ortep view of complex 2.

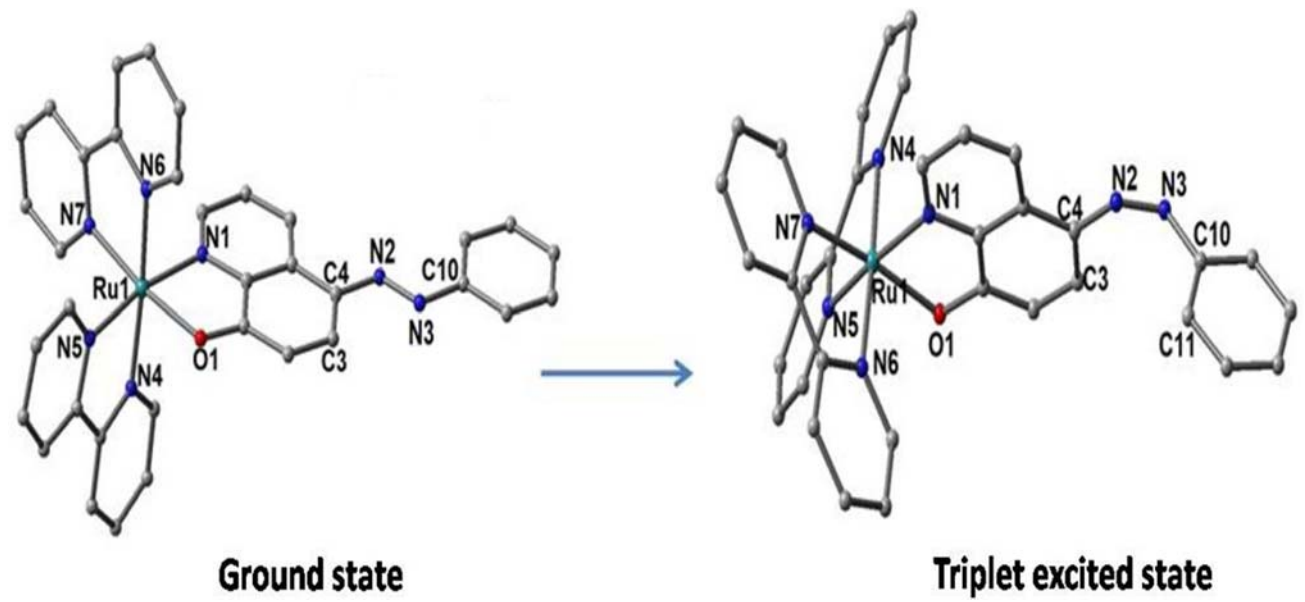

Figure 8. Geometrical optimization structure at S_0 state (left hand side) and T_1 state (right hand side) of complex **1**.

N coordinating monoanionic ligand. The N2–N3 distance is 1.252(10) Å for complex **1** and 1.261(4) Å for complex **2** suggesting free azo moiety. The Ru1–N1 and Ru1–O1 bond of 8-quiolinol moiety emerge at 2.050(7) Å and 2.061(6) Å, respectively for complex **1** and for complex **2** the distances are 2.066(2) Å and 2.092(2) Å, respectively. The dihedral angle through azo bond between 8-hydroxyquinoline and phenyl

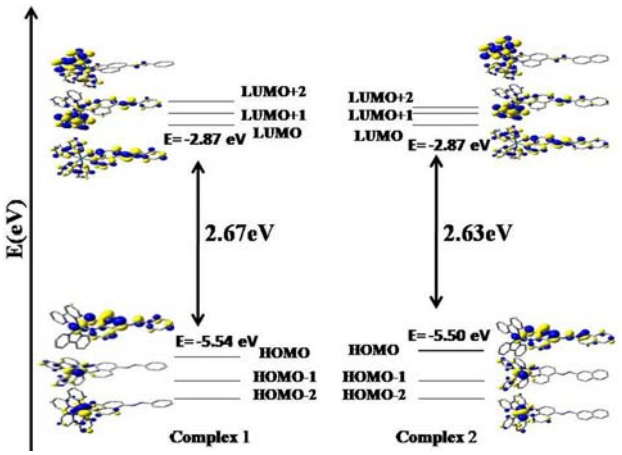

Figure 9. Partial molecular orbital diagram with some isodensity frontier molecular orbital of the complex. The vertical arrow indicates the HOMO−LUMO energy gap.

ring, C4–N2–N3–C10 is 178.8°(9) for complex **1** and 177.9°(3) for complex 2 suggests that the two moiety remains in trans position in the complexes. The geometry around the Ru(II) metal centres are distorted octahedral for both the complexes and those are considered by N6–Ru1–N4 bond angle of 175.1(3)° for complex **1** and 172.85(10) ° for complex **2**, respectively. Also the N7–Ru1–O1 bond angle of 171.8(3) ° for complex **1** and 170.80(9)° for complex **2** justified distorted octahedral geometry. The molecular views of the crystals are shown in Figures 6 and 7 and selected bond parameters are listed in Supplementary Information, Table S2 and Table S3 (Supplementary Information).

3.6 *Computational studies*

3.6a *Geometry optimization*: The diamagnetic nature of the complexes demonstrated their singlet ground state t_{2g}^6. The geometry optimization for all the complexes were performed in solution phases for both ground singlet (S_0) and lowest lying excited triplet (T_1) spin state. The optimized structures in both the states of complex **1** are given in Figure 8 and that of complex **2** in Supplementary Information (Figure S1, Supplementary Information). The ground state HOMO-LUMO energy calculation revealed that introduction of naphthyl group in complex **2** did not affect the LUMO energy but the HOMO energy increased slightly. Thus HOMO-LUMO energy gap (2.63 eV) in complex **2** decreased by an amount of energy 0.04 eV than the energy gap in complex **1** (2.67 eV) (Figure 9). In the complexes, the calculated bond parameters were in good agreement with the experimental values with distorted octahedral geometry and the slight discrepancy may be due to the crystal lattice distortion existing in real molecules. There was also very less difference in the geometrical parameters between ground state and triplet state, the main interesting difference was observed only in dihedral angle containing azo (-N=N-) bond. The dihedral angle was changed from ~ 179° to ~ 110° for both the complexes, and it means that the aryl fragment turned to cis geometry with 8-hydroxyquinoline fragment on excitation. The change for complex **1** is shown in Figure 8 and that of complex **2** in Supplementary Information (Figure S1). The selected

Table 2. Main calculated optical transition for complex **1** with composition in terms of molecular orbital contribution of the transition, vertical excitation energies, and oscillator strength in dichloromethane.

Complex 1

Transition	composition	E(ev)	Oscillator strength(f)	C.I	λ_{theo}	λ_{expt}	Assignment
$S_0 \rightarrow S_5$	H → L	2.3998	0.0797	0.13524	517	516	MLCT
	H-1 → L			0.35359			
	H-1 → L + 2			0.34065			
	H → L + 1			0.20783			
$S_0 \rightarrow S_{14}$	H-3 → L	3.0065	0.0296	0.33006	412	410	MLCT + LLCT
	H-3 → L + 1			0.12605			
	H-3 → L + 2			0.46537			
	H-2 → L + 2			0.15366			
	H → L + 4			0.25340			
$S_0 \rightarrow S_{32}$	H-3 → L + 3	3.6498	0.3960	0.23243	339	340	MLCT + ILCT + LLCT
	H-2 → L + 7			0.35606			
	H → L + 13			0.11521			
$S_0 \rightarrow S_{46}$	H-7 → L	4.2577	0.0284	0.24609	291	290	LLCT + ILCT
	H-2 → L + 8			0.49105			
	H-1 → L + 8			0.10422			

Table 3. Main calculated optical transition for complex **2** with composition in terms of molecular orbital contribution of the transition, vertical excitation energies, and oscillator strength in dichloromethane.

Complex 2							
Transition	Composition	E(ev)	Oscillator strength(f)	C.I	λ_{theo}	λ_{expt}	Assignment
$S_0 \rightarrow S_5$	H-3 → L + 2	2.3906	0.0743	0.10600	519	524	MLCT
	H-1 → L			0.33053			
	H-1 → L + 2			0.40822			
	H → L			0.10285			
	H → L + 1			0.17701			
$S_0 \rightarrow S_{14}$	H-3 → L + 1	2.9701	0.0023	0.17418	417	416	MLCT + LLCT
	H → L + 4			0.64520			
$S_0 \rightarrow S_{27}$	H-5 → L + 1	3.5306	0.0748	0.11891	351	351	MLCT + LLCT
	H-1 → L + 7			0.55358			
$S_0 \rightarrow S_{49}$	H-6 → L + 1	4.1811	0.0220	0.63895	296	290	LLCT

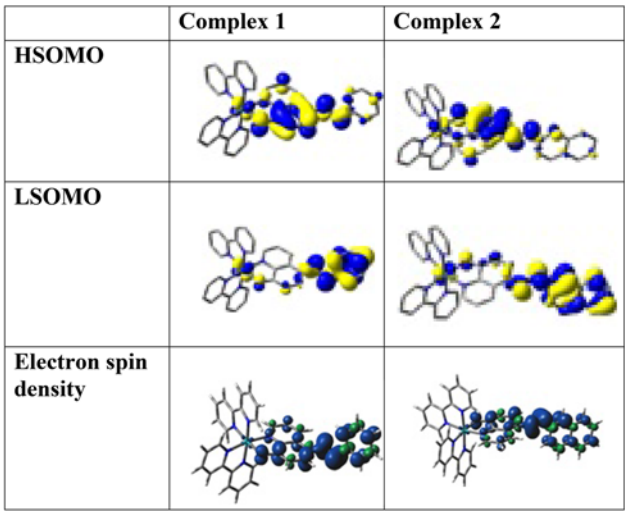

Figure 10. Isodensity surface (iso-cutoff= 0.03) plots of the highest and lowest singly occupied molecular orbitals, HSOMO and LSOMO, respectively, along with the corresponding electron spin density, for the complexes **1**, and **2** at their T_1 state geometry.

geometrical parameters for both ground and triplet state for the two complexes are given in Supplementary Information (Table S4, Supplementary Information).

3.6b *Absorption spectral analysis*: TD-DFT calculations matched well with the experimental absorption spectra. The lowest energy absorption bands (516 nm for complex **1** and 524 nm for complex **2**) were assigned mainly to the MLCT transition. The other low energy bands of complex **1** (410 nm, 340 nm) and complex **2** (416 nm, 351 nm) were due to a combination of MLCT and ILCT or LLCT transition. The higher energy absorptions around 290 nm for both the complexes were mainly due to the LLCT and ILCT transition.The slight bathochromic shift in absorbance in complex **2** resulted from extended π-conjugation in comparison to complex **1**. From the partial frontier molecular orbital compositions and energy levels of the complexes, listed in Supplementary Information. (Table S5 and Table S6, Supplementary Information) and natural transition orbitals (NTOs) analysis (Supplementary Information, Table S7 and Table S8, respectively for complex **1** and **2**) the nature of absorption bands were assigned. The calculated absorption energies associated with their oscillator strengths, the main configurations and their assignments as well as the experimental results are given in Table 2 for complex **1** and in Table 3 for complex **2**.

3.6c *Emission spectral analysis*: TD-DFT studies at T_1 state for the complexes were thoroughly studied which revealed that the photoluminescence in complexes mainly originated from ligand centered triplet state charge transfer transitions. The isodensity surfaces of the highest and lowest singly occupied molecular orbitals, namely HSOMO and LSOMO for all species, at the unperturbed T_1 geometry are plotted in Figure 10. In HSOMO electron density resides on the π orbital of 8-hydroxyquinoline moiety. On the other hand, azoaryl part contributed to LSOMO. The total spin density plot at T_1 state illustrated that the spin density was mainly localized on the of 8-hydroxyquinoline and azoaryl moiety. This data corroborated with mainly ^{3}ILCT or ^{3}LLCT type transitions for both the complexes.

4. Conclusions

Herein we reported synthesis, crystal structures, photophysical properties of two monomeric heteroleptic Ru(II) complexes in combination with bpy and 8-oxyquinololate azo ligands. The synthesized

complexes exhibited promising light-responsive behavior in presence of external stimuli such as UV light exposure. There was remarkable colour change by which the geometry change can be ascertained and also a significant alteration in the absorption band upon UV light irradiation was noticed. Most of the experimental outcomes were well-supported by theoretical calculations.

Supplementary Information (SI)

X-ray crystallographic file in CIF format for complex 1 and complex 2 having CCDC reference number 1998590 and 1998672, respectively.

Acknowledgements

R. P. acknowledges CSIR, New Delhi for Funding and Department of Chemistry, Jadavpur University for infrastructure and support. K.K.R. acknowledges RUSA 2.0, Department of Chemistry, Jadavpur University for funding and support.

Conflict of interest The authors declare no conflict of interest in the work presented in the manuscript.

References

1. Huang X and Li T 2019 Recent progress in the development of molecular-scale electronics based on photoswitchable molecules *J. Mater. Chem. C* **8** 821
2. Weber C, Liebig T, Gensler M, Zykov A, Pithan L, Rabe J P, Hecht S, Bléger and Kowarik S 2016 Cooperative Switching in Nanofibers of Azobenzene Oligomers *Sci. Rep.* **6** 25605
3. Dhammika B H M and Burdette S C 2012 Photoisomerization in different classes of azobenzene *Chem. Soc. Rev.* **41** 1809
4. Yamamura M, Okazaki Y and Nabeshima T 2012 Photoisomerization locking of azobenzene by formation of a self-assembled macrocycle *Chem. Commun.* **48** 5724
5. Wazzan N A, Richardson P R and Jones A C2010 *Cis-Trans* isomerisation of azobenzenes studied by laser-coupled NMR spectroscopy and DFT calculations *Photochem. Photobiol. Sci.* **9** 968
6. Schultz T, Quenneville J, Levine B, Toniolo A, Martínez T J, Lochbrunner S, Schmitt M, Shaffer J P, Zgierski M Z and Stolow A 2003 Mechanism and Dynamics of AzobenzenePhotoisomerization *J. Am. Chem. Soc.* **125** 8098
7. Cembran A, Bernardi F, Garavelli M, Gagliardi L and Orlandi G 2004 On the Mechanism of the cis-trans Isomerization in the Lowest Electronic States of Azobenzene: S0, S1, and T1 *J. Am. Chem. Soc.* **126** 3234
8. Pérez-Miqueo J, Altube A, García-Lecina E, Tron A, McClenaghanc N D and Freixa Z 2016 Photoswitchableazobenzene-appended iridium(III) complexes *Dalton Trans*. **45** 13726
9. Kume S, Kurihara M and Nishihara H 2001 Reversible *trans–cis* photo isomerization of azobenzene-attached bpyridine ligands coordinated to cobalt using a single UV light source and the Co(III)/Co(II) redox change *Chem. Commun.* 1656
10. Hasheminasab A, Wang L, Dawadi M B, Bass J, Herrick R S, Rack J J and Ziegler C J 2015 Induction of E/Z isomerization in a pendant metal-bound azobenzene: a synthetic, spectroscopic and theoretical study *Dalton Trans*. **44** 15400
11. Yin T-T, Zhao Z-X and Zhang H-X 2016 Theoretical study of the cis–trans isomerisation mechanism of a pendant metal-bound azobenzene *RSC Adv*. **6** 79879
12. Amar A, Savel P, Akdas-Kilig H, Katan C, Meghezzi H, Boucekkine A, Malval J P and Fillaut J L 2015 Photoisomerisation in Aminoazobenzene-Substituted Ruthenium(II) Tris(bpyridine) Complexes: Influence of the Conjugation Pathway *Chem. Eur. J.* **21** 8262
13. Moustafa M E, McCready M S and Puddephatt R J 2012 Switching by Photochemical trans−cis Isomerization of Azobenzene Substituents in Organo platinum Complexes *Organometallics* **31** 6262
14. (a) Maity A, Bera S and Rajak K K 2019 Synthesis and comparative studies of photophysical and electrochemical properties of three different types of new heteroleptic 5-arylazo-8-hydroxyquinoline complexes of rhodium including trans → cis isomerism studies *J. Organomet. Chem.* **887** 48; (b) Maity A and Rajak K K 2019 Photo induced trans → cis isomerism studies of heteroleptic iridium complex with 8-quinolinol-5-phenylazo ligand: Photophysical and electrochemical studies and it's theoretical investigations *J. Mol. Struct.* **1181** 38
15. Otsuki J, Suwa K, Sarker K K and Sinha C 2007 Photoisomerization and Thermal Isomerization of Arylazoimidazoles *J. Phys. Chem. A* **111** 1403
16. Doucet H, Ohkuma, T, Murata K, Yokozawa T, Kozawa M, Katayama E, England A F, Ikariya T and Noyori R 1998 Trans-[RuCl2 (phosphane) 2 (1, 2-diamine)] and Chiral trans-[RuCl2 (diphosphane) (1, 2-diamine)]: Shelf-Stable Pre catalysts for the Rapid, Productive, and Stereo selective Hydrogenation of Ketones *Angew. Chem., Int. Ed.* **37** 1703
17. Clapham S E, Hadzovic A and Morris R H 2004 Mechanisms of the H 2-hydrogenation and transfer hydrogenation of polar bonds catalyzed by ruthenium hydride complexes *Coord. Chem. Rev.* **248** 2201
18. Kamigaito M, Ando T and Sawamoto M 2001 Metal-catalyzed living radical polymerization *Chem. Rev.* **101** 3689
19. De Sousa S, Lyu S, Ducasse L, Toupance T and Olivier C 2015 Tuning visible-light absorption properties of Ru-diacetylide complexes: simple access to colorful efficient dyes for DSSCs *J. Mater. Chem. A* **3** 18256
20. Pashaei B, Shahroosvand H, Graetzel M and Nazeeruddin M K 2016 Influence of Ancillary Ligands in Dye-Sensitized Solar Cells *Chem. Rev.* **116** 9485
21. Nazeeruddin M K, Zakeeruddin S, Lagref J-J, Liska P, Comte P, Barolo C, Viscardi G, Schenk K and Grätzel

M 2004 Stepwise assembly of amphiphilic ruthenium sensitizers and their applications in dye-sensitized solar cell *Coord. Chem. Rev.* **248** 1317
22. Khatua S, Samanta D, Bats J W and Schmittel M 2012 Rapid and Highly Sensitive Dual-Channel Detection of Cyanide by BisheterolepticRuthenium(II) Complexes *Inorg. Chem.* **51** 7075
23. Chao H, Zhang P and Ji L 2013 Preparation method and application of anthraquinone polypyridine ligand and ruthenium-anthraquinone complex. Patent CN103012401A
24. Geletii Y V, Huang Z, Hou Y, Musaev D G, Lian T and Hill C L 2009 Homogeneous light-driven water oxidation catalyzed by a tetraruthenium complex with all inorganic ligands *J. Am. Chem. Soc.* **131** 7522
25. Concepcion J J, Tsai M-K, Muckerman J T and Meyer T J 2010 Mechanism of water oxidation by single-site ruthenium complex catalysts *J. Am. Chem. Soc.* **132** 1545
26. Limburg B, Bouwman E and Bonnet S 2016 Rate and Stability of Photocatalytic Water Oxidation using [Ru(bpy)3]2+ as Photosensitizer *ACS Catal.* **6** 5273
27. Zhu B-Z, Chao X-J, Huang C-H and Li Y 2016 Delivering the cell impermeable DNA 'light-switching' Ru (ii) complexes preferentially into live-cell nucleus via an unprecedented ion-pairing method *Chem. Sci.* **7** 4016
28. Pierroz V, Rubbiani R, Gentili C, Patra M, Mari C, Gasser G and Ferrari S 2016 Dual mode of cell death upon photo-irradiation of a RuIIpolypyridyl complex in interphase or mitosis *Chem. Sci.* **7** 6115
29. Boynton A N, Marcélis L and Barton J K 2016 [Ru$(Me_4phen)_2dppz]^{2+}$, a Light Switch for DNA Mismatches *J. Am. Chem. Soc.* **138** 5020
30. Erkkila K E, Odom D T and Barton J K 1999 Recognition and reaction of metallo intercalators with DNA *Chem. Rev.* **99** 2777
31. Lo K K-W, Hui W-K, Chung C-K, Tsang K H-K, Ng D C-M, Zhu N and Cheung K-K 2005 Biological labelling reagents and probes derived from luminescent transition metal polypyridine complexes *Coord. Chem. Rev.* **249** 1434
32. (a) Khatua S, Samanta D, Bats J W and Schmittel M 2012 Rapid and Highly Sensitive Dual-Channel Detection of Cyanide by BisheterolepticRuthenium(II) Complexes *Inorg. Chem.* **51** 7075; (b) Das, A, Kundu T, Mobin S M, Priego J L, Jimenez-Aparicio R and Lahiri G K 2013 Influence of ancillary ligands on the electronic structure and anion sensing features of ligand bridged diruthenium complexes *Dalton Trans.* **42** 13733
33. (a) Yue X, Zhu Z, Zhang M and Ye Z 2015 Reaction-Based Turn-on Electrochemiluminescent Sensor with a Ruthenium(II) Complex for Selective Detection of Extracellular Hydrogen Sulfide in Rat Brain *Anal. Chem.* **87** 1839; (b) Li M-J, Wong K M-C, Yi C and Yam V W-W 2012 New Ruthenium(II) Complexes Functionalized with Coumarin Derivatives: and Imaging Studies *Chem. Eur. J.* **18** 8724
34. Zheng Z-B, Wu Y-Q, Wang K-Z and Li F 2014 pH luminescence switching, dihydrogen phosphate sensing, and cellular uptake of a hetero bimetallic ruthenium(II)-rhenium(I) complex *Dalton Trans.* **43** 3273
35. Johansson O, Johannissen L O and Lomoth R 2009 Bistable Molecular Switches Based on Linkage Isomerization in Ruthenium Polypyridyl Complexes with a Ligand-Bound Ambidentate Motif *Chem. Eur. J.* **15** 1195
36. Bhattacharya S 1993 8-Quinolinolate complexes of ruthenium(ii). Synthesis, characterization and electron transfer properties *Polyhedron* **12** 235
37. Jia W-G, Cheng M-X, Xu Q-T, Gao L-L and Yuan G 2018 Synthesis of six 8-quinolinate-based ruthenium complexes with high catalytic activity for nitroarene reduction *Polyhedron* **153** 69
38. Meng T, Qin Q, Chen Z, Zou H, Wanga K and Liang F 2019 Dicsoveryof high in vitro and in vivo antitumor activities of organometallic ruthenium(II)-arene complexes with 5,7-dihalogenated-2-methyl-8-quinolinol *Dalton Trans.* **48** 5352
39. Kubanik M, Holtkamp H, Söhnel T, Jamieson S M F and Hartinger C G 2015 Impact of the Halogen Substitution Pattern on the Biological Activity of Organoruthenium 8-Hydroxyquinoline Anticancer Agents *Organometallics* **34** 5658
40. Kaulage M H, Maji B, Pasadi S, Bhattacharya S and Muniyappa K 2017 Novel ruthenium azo-quinoline complexes with enhanced photonuclease activity in human cancer cells *Eur. J. Med. Chem.* **139** 1016
41. Sarkar R, Mondal P and Rajak K K 2014 Synthesis, structure and spectroscopic properties of Re(i) complexes incorporating 5-arylazo-8-hydroxyquinoline: a density functional theory/time-dependent density functional theory investigation *Dalton Trans.* **43** 2859
42. Godwin J B and Meyer T J 1971 Nitrosyl-nitrite interconversion in ruthenium complexes *Inorg. Chem.* **10** 2150
43. Deda M L, Grisolia A, Aiello I, Crispini A, Ghedini M, Belviso S, Amati M and Lelj F 2004 Investigations on the electronic effects of the peripheral 4′-group on 5-(4′-substituted)phenylazo-8-hydroxyquinoline ligands: zinc and aluminium complexes *Dalton Trans.* 2424
44. Valuer B 2001 In *Molecular Fluorescence: Principle and Applications* (Weinheim: Wiley-VcH)
45. Runge E and Gross E K U 1984 Density-Functional Theory for Time-Dependent Systems *Phys. Rev. Lett.* **52** 997
46. (a) Becke A D 1993 Density-functional thermochemistry. III. The role of exact exchange *J. Chem. Phys.* **98** 5648; (b) Lee C, Yang W and Parr R G 1988 Development of the Colle-Salvetti correlation-energy formula into a functional of the electron density *Phys. Rev. B* **37** 785
47. (a) Barone V and Cossi M 1998 Quantum Calculation of Molecular Energies and Energy Gradients in Solution by a Conductor Solvent Model *J. Phys. Chem. A* **102** 1995; (b) Cossi M and Barone V 2001 Time-dependent density functional theory for molecules in liquid solutions *J. Chem. Phys.* **115** 4708; (c) Cossi M, Rega N, Scalmani G and Barone V 2003 Energies, Structures, and Electronic Properties of Molecules in Solution with the C-PCM Solvation Model *J. Comp. Chem.* **24** 669
48. (a) Casida M E, Jamoroski C, Casida K C and Salahub D R 1998 Molecular excitation energies to high-lying bound states from time-dependent density-functional

response theory: Characterization and correction of the time-dependent local density approximation ionization threshold *J. Chem. Phys.* **108** 4439; (b) Stratmann R E, Scuseria G E and Frisch M J 1998An efficient implementation of time-dependent density-functional theory for the calculation of excitation energies of large molecules *J. Chem. Phys*. **109** 8218; (c) Bauernschmitt R and Ahlrichs R 1996 Treatment of electronic excitations within the adiabatic approximation of time dependent density functional theory *Chem. Phys. Lett*. **256** 454

49. Hay P J and Wadt W R 1985 *J. Chem. Phys*. **82** 299
50. Frisch M J, Trucks G W, Schlegel H B, Scuseria G E, Robb M A, Cheeseman J R, Scalmani G, Barone V, Mennucci B, Petersson G A, Nakatsuji H, Caricato M, Li X, Hratchian H P, Izmaylov A F, Bloino J, Zheng G, Sonnenberg J L, Hada M, Ehara M, Toyota K, Fukuda R, Hasegawa J, Ishida M, Nakajima T, Honda Y, Kitao O, Nakai H, Vreven T, Montgomery Jr J A, Peralta J E, Ogliaro F, Bearpark M, Heyd J J, Brothers E, Kudin K N, Staroverov V N, Kobayashi R, Normand J, Raghavachari K, Rendell A, Burant J C, Iyengar S S, Tomasi J, Cossi M, Rega N, Millam J M, Klene M, Knox J E, Cross J B, Bakken V, Adamo C, Jaramillo J, Gomperts R, Stratmann R E, Yazyev O, Austin AJ, Cammi R, Pomelli C, Ochterski J W, Martin R L, Morokuma K, Zakrzewski V G, Voth G A, Salvador P, Dannenberg J J, Dapprich S, Daniels A D, Farkas Ö, Foresman J B, Ortiz J V, Cioslowski J and Fox D J 2009 *Gaussian 09, (Revision A.1),Gaussian, Inc., Wallingford, CT*
51. O'Boyle N M, Tenderholt A L and Langner K M 2008 Cclib: A Library for Package-Independent Computational Chemistry Algorithms *J. Comp. Chem.* **29** 839
52. SMART; SAINT; SADABS; XPREP; SHELXTL 1998 *Bruker AXS Inc. Madison WI*
53. Sheldrick G M 2003 *SHELXTL, v.6.14, Bruker AXS Inc. Madison WI*
54. Johnson C K 1976 *ORTEP Report ORNL-5138*, Oak Ridge National Laboratory, Oak Ridge TN
55. Macrae C F, Edgington P R, McCabe P, Pidcock E, Shields G P, Taylor R, Towler M and van de Streek J 2006 Mercury: Visualization and Analysis of Crystal Structures *J. Appl. Cryst.* **39** 453
56. (a) Alauddin S M, Aripin N F K, Velayutham T S, Chaganava I and Martinez-Felipe A 2019 The role of conductivity and molecular mobility on the photoanisotropic response of a new azo-polymer containing sulfonic groups *J. Photochem. Photobiol. A Chem.* **389** 112268; (b) Kumar G S and Neckers D C 1989 Photochemistry of azobenzene-containing polymers *Chem. Rev.* **89** 1915; (c) Cho E N, Zhitomirsky D, Han G G D, Liu Y and Grossman J C 2017 Molecularly Engineered Azobenzene Derivatives for High Energy Density Solid-State Solar Thermal Fuels *ACS Appl. Mater. Interf.* **9** 8679
57. (a) Jasimuddin S K, Byabartta P, Mostafa G, Liou J-C, Lu T-H and Sinha C 2004 The synthesis, spectroscopic properties and electrochemistry of (8-quinolinolato)-bis-{1-alkyl-2- (arylazoimidazole)}ruthenium(ii) hexafluorophosphate: single crystal X-ray structure of [ru(q)(meaaime)2](PF_6)CH_2Cl_2[Q = 8-quinolinolate, meaaime = 1-methyl-2-(p-tolylazoimidazole)] *J. Coord. Chem.* **57** 75; (b) Misra T K and Sinha C 1999 Synthesis, spectral characterization and redox properties of ruthenium(II) complexes with $RuN_2P_2Cl_2$ coordination spheres *IJC-A* **38A** 346